Adapting Temperature Predictions to MR Imaging in Treatment Position to Improve Simulation-Guided Hyperthermia for Cervical Cancer

Iva VilasBoas-Ribeiro [ORCID], Kemal Sumser [ORCID], Sven Nouwens [ORCID], Theresa Feddersen [ORCID], W.P.M.H. Heemels [ORCID], Gerard C. van Rhoon [ORCID], and Margarethus M. Paulides [ORCID], *Senior Member, IEEE*

Abstract—**Hyperthermia treatment consists of elevating the temperature of the tumor to increase the effectiveness of radiotherapy and chemotherapy. Hyperthermia treatment planning (HTP) is an important tool to optimize treatment quality using pre-treatment temperature predictions. The accuracy of these predictions depends on modeling uncertainties such as tissue properties and positioning. In this study, we evaluated if HTP accuracy improves when the patient is imaged inside the applicator at the start of treatment. Because perfusion is a major uncertainty source, the importance of accurate treatment position and anatomy was evaluated using different perfusion values. Volunteers were scanned using MR imaging without ("planning setup") and with the MR-compatible hyperthermia device ("treatment setup"). Temperature-based quality indicators were used to assess the differences between the standard, apparent and the optimized hyperthermia dose. We conclude that pre-treatment imaging can improve HTP predictions accuracy but also, that tissue perfusion modelling is crucial if temperature-based optimization is applied.**

Index Terms—**Hyperthermia treatment planning (HTP), MR imaging, thermal modeling, perfusion, optimization approach.**

Impact Statement—**Changes in anatomy and position influence the HTP's predictive value. SAR-based optimization was more robust than temperature-based optimization to variations in anatomy, position, and perfusion.**

I. INTRODUCTION

HYPERTHERMIA treatment consists of elevating the tumor's temperature to 39-44 °C to enhance the effect of chemotherapy and radiotherapy without adding toxicity to the healthy tissue [1], [2]. The efficacy of hyperthermia depends on achieving high temperatures in the tumor region while maintaining low temperatures in the healthy tissue. Several clinical trials [3], [4] demonstrated a thermal-dose effect relationship emphasizing the importance of precise heat delivery to improve hyperthermia treatment efficacy. The control and adaptation of steering settings to improve the quality of treatment are currently based on temperature monitoring and complaint-adaptive hyperthermia treatment planning (HTP). Although this tool has been used in clinical practice, its accuracy and predictive value is highly dependent on modeling uncertainties, such as positioning, anatomy, and tissue properties.

In clinical practice, computed tomography (CT) or magnetic resonance imaging (MRI) are used to capture the patient's anatomy as a basis for a patient-specific treatment plan. These images are usually taken at least a week before treatment and without the real treatment device present. As a consequence, patient position and anatomy are different, resulting in possible deviations between planned and actual applied hyperthermia dose distributions. Few studies have used the MR-compatible device in combination with MRI to suggest that accuracy of HTP was optimum if the patient was imaged in the actual treatment position [5], [6], [7]. This framework allowed to create an

MR-based HTP and show that position and anatomy deviations can impact HTP predictive value [6], [8]. Though, these analyses were mainly based on SAR-based analysis, and consequently, the true benefit of pre-treatment imaging in treatment position on the applied temperature is an open question.

One of the main challenges in temperature predictions is dealing with perfusion uncertainties. These uncertainties can alter the reliability of the predictions, limiting the confidence in their use for treatment guidance. Canters et al. [9] indicated that uncertainties in thermal parameters (the temperature of 10%, 50%, and 90% of the HTV, T10, T50, and T90, respectively) could lead to 0.2 °C–0.4 °C decreases in T50 and T90. De Greef et al. [10] showed that perfusion uncertainties could cause temperature deviations of 1 °C. Hence, perfusion is a well-established source of uncertainty that can modify temperature predictions [11], [12], [13]. Modeling perfusion is challenging since perfusion is a response to thermoregulation and differs between tissues and individual patients [14], [15]. As perfusion is difficult to model, any temperature prediction accuracy assessment should include perfusion uncertainties to understand its effects on temperature predictions.

During HTP, the steering settings of the hyperthermia device are optimized to maximize the predicted heat delivery in the tumor without overheating healthy tissues. Precise steering to avoid hotspots is of great importance since increasing tumor temperature to the therapeutic level is only possible if the patient's tolerance is not exceeded [6], [16], [17]. Optimization of the device settings can be based on temperature or SAR distribution. A clinical study comparing SAR-based and temperature-based steering has not been possible yet due to the immense challenge of obtaining sufficient and accurate temperature information on tumor and healthy tissues in patients. Hence, the optimal choice between these two options has not yet been established and is still an open debate. Canters et al. [9] have shown that SAR-based optimization is equally effective in optimizing thermal dose as temperature optimization. At the same time, de Greef et al. [10], [12] found that temperature-based optimization is superior under variation of perfusion values. In the recent ESHO benchmarks [18], it is suggested to perform both optimizations when investigating and comparing HTP predictions to improve treatment delivery.

In this modeling study, we assessed how changes in anatomy and position can affect the accuracy of temperature predictions. Additionally, we investigated the potential benefits of incorporating precise treatment anatomy and position data to improve treatment delivery. These evaluations were conducted for both SAR and temperature- based optimization approaches, and for different perfusion schemes.

II. MATERIALS AND METHODS

A. MRI Acquisition and Protocol

In this study, we collected data from 14 healthy female volunteers. The institutional review board approved this study using the protocol (MEC-2014-096). All volunteers were positioned inside the BSD-2000-3D MR compatible system (Pyrexar Medical Cop., Salt Lake City, UT, USA) [19], [20], which
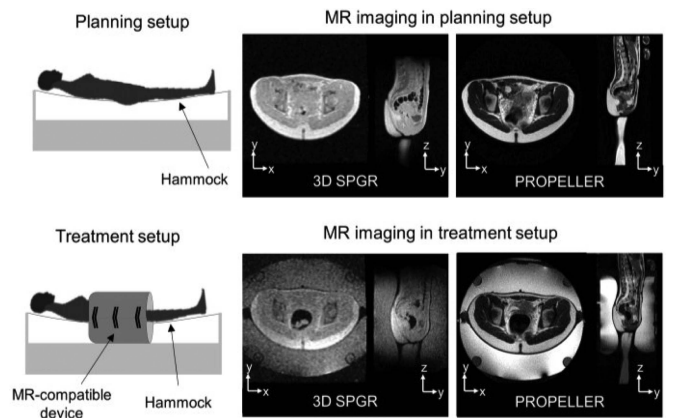
Fig. 1. Volunteer experiment setup: schematic representation of the volunteer in the planning and treatment setup, and the MR images taken at each setup. The column of the MR imaging represents the 3D SPGR images, and the second column denotes the images acquired using PROPELLER.
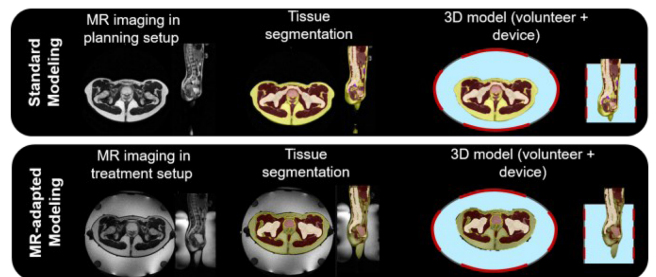
Fig. 2. Schematic illustration of the process of creating the modeling in the HTP process. The MR images taken in planning setup were used to generate the standard modeling, whereas the MR images at the treatment setup were used to create the MR-adapted modeling.

is integrated into a 1.5T GE Optima 450W scanner (General Electric Healthcare, Waukesha, WI, USA).

As shown in Fig. 1, we took MR images of the volunteers in the planning and treatment setup. The planning setup intends to mimic the imaging setup used for the current HTP, and the treatment setup reproduces the hyperthermia treatment. Regarding the MR imaging protocol, we used the 3D spoiled gradient recalled echo (SPGR) pulse sequence to visualize gastrointestinal air and the PROPELLER sequence to obtain high-resolution anatomic images. The details about the experiment and the MR protocol can be found in our previous work [21].

B. Hyperthermia Treatment Planning

1) Patient Model Generation: The MR images were segmented into bone, muscle, gastrointestinal air, and fat. The tissue segmentation was based on thresholding combined with manual segmentation on the MR images shown in Fig. 1. The software used for this process was MIM Maestro (MIM Software Inc. USA). Furthermore, a gross target volume (GTV) and a hyperthermia target volume (HTV) were added. Fig. 2 summarizes the main steps to generate the 3D model. The standard modeling denotes the clinical procedure where the modeling is based on imaging without the hyperthermia device. The volunteer

TABLE I
LITERATURE VALUES OF EM AND THERMAL TISSUE PROPERTIES FOR THERMAL SIMULATIONS

Material	ε_r[-]	σ [S/m]	c [J/kg/°C]	K [W/m/°C]	Q [W/kg]	ρ [kg/m³]	ω [ml/min/kg] St B	ω [ml/min/kg] Bas.	ω [ml/min/kg] St A
Shell	2.8	0.004	-	-	-	1180	-	-	-
Waterbolus	80.95	0.0026	-	-	-	1000	-	-	-
Bone	15.3	0.0643	1313	0.32	0.15	1908	10	10	10
Muscle	66.0	0.708	3421	0.45	0.96	1090	188.7	37	300
Internal air			10040	0.03	-	1	-	-	-
Fat	12.7	0.0684	2348	0.21	0.51	911	69.0	33	200
GTV	70.0	0.75	3950	0.51	-	1050	94.4 ($0.5 \times \omega_{muscle}$)	189 ($5.1 \times \omega_{muscle}$)	80 ($0.27 \times \omega_{muscle}$)

The perfusion values given in different color were used for the robustness evaluation.

positioning was done using the clinical standard approach that consists in verifying the distances between the hyperthermia device and patient. The MR-adapted modeling is based on accurate treatment anatomy and position since the volunteer was scanned inside the hyperthermia device including filled water bolus. This modeling intends to replicate the procedure where the modeling is adapted to the MR images taken at start of the treatment.

2) Electromagnetic and Temperature Calculations: The electromagnetic (EM) field for each antenna was calculated using the Finite-Difference-Time-Domain (FDTD) solver in Sim4life (v6.2 Zurich MedTech AG, Zurich, Switzerland). The details about the EM simulations are given in our previous work [21]. Furthermore, we computed the 3D steady-state temperature distributions using the Pennes' Bio-Heat Equation, which formulation is given in (1) [22], in Sim4life.

$$\rho c \frac{\partial T}{\partial t} = \nabla \left(k \, \nabla T \right) + \rho Q_m + \rho S - \rho_b c_b \rho \omega \left(T - T_b \right) \quad (1)$$

where T [°C] is the temperature, t [min] is the time, c [J kg^{-1}°C^{-1}] is the specific heat capacity, ρ[kg m^{-3}] is the volume density of mass, k[W m^{-1}°C^{-1}] is the thermal conductivity, ω [mlmin^{-1}kg^{-1}] is the volumetric blood perfusion, Q_m [W kg^{-1}] is the metabolic heat generation, S [W kg^{-1}] is the SAR, which serves as a source for the thermal simulations, and the subscript b denotes blood properties. Note that in steady state ∂T/∂t is equal to 0. Energy losses were modeled using a mix of convective boundary conditions at the interfaces of the skin and water bolus, where the heat transfer coefficient was equal to 40 W m^{-2}°C^{-1} [9]. The initial temperature in tissues was set to 37 °C and the temperature of the water bolus was set at 20 °C

The dielectric properties at 100 MHz and thermal tissue properties are listed in Table I [23]. Perfusion at thermal stress conditions was considered for all tissues except bone [23]. Since tumor properties at baseline condition were unavailable, we calculated the perfusion value at 37 °C based on the temperature-dependent perfusion relation suggested by Lang et al. [11]. For each perfusion value set, a temperature-based optimization was performed.

3) Optimization: We conducted two types of optimizations to remove a possible bias in our results. SAR-based optimization was implemented by using the clinical software at Erasmus MC (VEDO) [24], [25]. The optimization implemented in VEDO
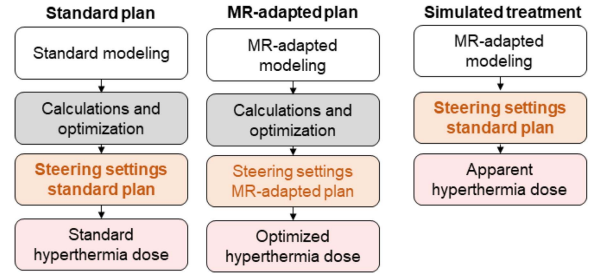
Fig. 3. Description of the treatment plans and the apparent hyperthermia dose during the simulated hyperthermia treatment. The modeling procedure of each treatment plan is explained in Fig. 2. Because two different optimizations were performed, six temperature distributions were acquired, where three correspond to the SAR-based optimization and other three correspond to the temperature-based optimization.

maximizes tumor-to-hotspot quotient (THQ), which formulation is given in (2).

$$THQ = \frac{\overline{SAR}_{HTV}}{\overline{SAR}_{hotspot}} \quad (2)$$

where SAR [W kg^{-1}] is the specific absorption rate, $\overline{SAR}_{HTV}$ is the average SAR within the HTV and $\overline{SAR}_{hotspot}$ is the average SAR in the hotspots, that is 50 ml of the healthy tissue with the highest SAR outside the HTV. The total input power was increased until a maximum temperature of 44 °C was achieved in all tissues [15].

The temperature-based optimization [26], [27] consisted of minimizing the following goal function (3).

$$J = \int_{p \in HTV} \left(\max \left(T_c - T \left(p \right), 0 \right) \right)^2 dp \quad (3)$$

where J is the goal function, T_c is the minimal desired tumor temperature of 43 °C, p corresponds to tissues within the HTV. The goal function is optimized subject to a general constraint that limits the temperature of normal tissue to 44 °C.

C. Definition of Treatment Plan and Hyperthermia Dose

Fig. 3 illustrates two plans for reproducing the current clinical practice and the desired treatment plan. To create the plan conducted in clinical practice, we used the volunteer's MR imaging

in the planning setup and developed a standard plan. The standard hyperthermia dose is the temperature prediction acquired using the standard plan's steering settings. Our second plan, the "MR-adapted plan," represents the optimized plan, as it is based on the patient's true treatment anatomy and position inside the hyperthermia device. This plan optimizes the steering settings on the treatment setup, and the acquired temperature predictions are named optimized hyperthermia dose. Finally, to understand the accuracy of the standard plan and the need for an MR-adapted plan, we simulated the delivery of the treatment. In this scenario, we applied the steering settings from the standard plan to the true treatment anatomy and position. The calculated temperature distributions are called "apparent hyperthermia dose".

D. Thermal Dosimetry Evaluation

We computed the difference in T10, T50, and T90 (ΔTx) between the plans and the apparent dose. These parameters correspond to the temperature of 10%, 50%, and 90% of the HTV [18], [28].

$$\Delta Tx_{\text{plan}}\,(^\circ C) = Tx_{plan} - Tx_{\text{apparent hyperthermia dose}} \quad (4)$$

To assess the differences between HTP predictions and administrated treatment, we quantified the absolute difference between standard plan and the apparent hyperthermia dose in the simulated treatment. Regarding the dosimetric evaluation between MR-adapted plan, we assess the improvement when the steering settings are optimized according to the treatment position and anatomy. Since thermal dose is related to treatment outcome [5], [29], we considered a change in temperature higher than 0.2 °C as clinically relevant.

E. Robustness Evaluation

This study intends to evaluate how robust the conclusions are, despite the optimization and perfusion values chosen. Hence, we used two perfusion values at thermal stress conditions (St.A and St.B) [18], [30], [31], [32], and one at baseline conditions (Bas) [23]. The perfusion schemes at thermal stress conditions were based on the most used values in literature and because these include perfusion tissue contrast. Hence, thermal simulations were conducted for each perfusion scheme and new optimization was performed. Table I presents the different perfusion values and the ratio between the perfusion of GTV and muscle. We conducted a Kruskal-Wallis analysis to evaluate if there were significant alterations in absolute error and benefit when using different perfusion values. The calculated absolute error and benefit for each perfusion set was inserted to the statistical test and the p-value for each comparison was calculated

III. RESULTS

A. Comparison Between Standard Hyperthermia Dose and Apparent Hyperthermia Dose

We first quantified the difference between the standard and apparent hyperthermia doses. The standard hyperthermia dose is optimized on the pre-treatment anatomy and the position. The apparent hyperthermia dose is when the standard plan settings
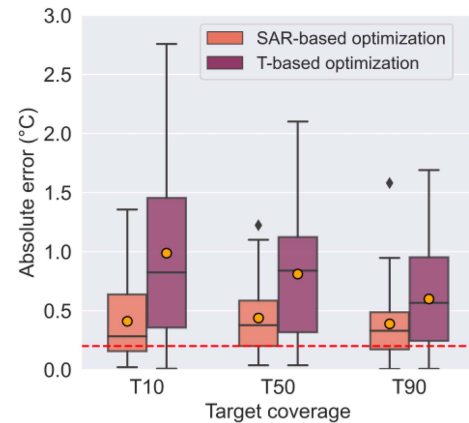

Fig. 4. Boxplot of the absolute error between the standard hyperthermia dose and the apparent hyperthermia dose using SAR- or T-based optimization. The inter-quartile range represents the middle 50% of the dataset where the top line represents 75% of the data below the upper quartile and the bottom line consists of 25% of the data below the lower quartile. The middle line represents the median, the colored circle represents the average of the data set and the diamond shaped markers represent the outliers. The red dotted line denotes the clinically relevant temperature difference (0.2 °C).

are applied on the patient's true treatment anatomy and position inside the device. The absolute error consists of the difference between the standard and apparent hyperthermia doses.

Fig. 4 shows the absolute error between standard and apparent hyperthermia dose when using perfusion values at thermal stress B (St. B). For |ΔT10|, |ΔT50| and |ΔT90|, the mean and standard deviation of the absolute error was 0.4±0.3 °C when including both optimization approaches. For temperature-based optimization, the absolute errors were substantially higher than for SAR-based optimization. The large absolute errors indicate that changes in anatomy and position decrease the predictive value of temperature predictions. The temperature parameters acquire used to calculate the absolute errors are illustrated in Fig. 5. These scatter plots (Fig. 5) show the temperature-based quality parameters for the standard, optimal and apparent hyperthermia dose using different optimizations. These parameters are based on temperature distributions acquired using perfusion values at thermal stress conditions B (St. B).

B. Evaluation of the Benefit of Including True Treatment Anatomy and Position in HTP

To evaluate the potential of including the treatment anatomy and position in HTP, we created a new HTP that was adapted to the imaging of the volunteer in the hyperthermia device. Since MRI enables to acquire the accurate treatment anatomy and position, this represents the optimized dose, hence, we named this HTP based on MR-adapted plan, optimized hyperthermia dose. The benefit of the MR-adapted plan is defined as the difference between the optimized hyperthermia dose and the apparent hyperthermia dose. Fig. 6 shows the benefit of using the MR-adapted plan when using perfusion values at St. B. For SAR-based optimization, the improvement in T90, T50,
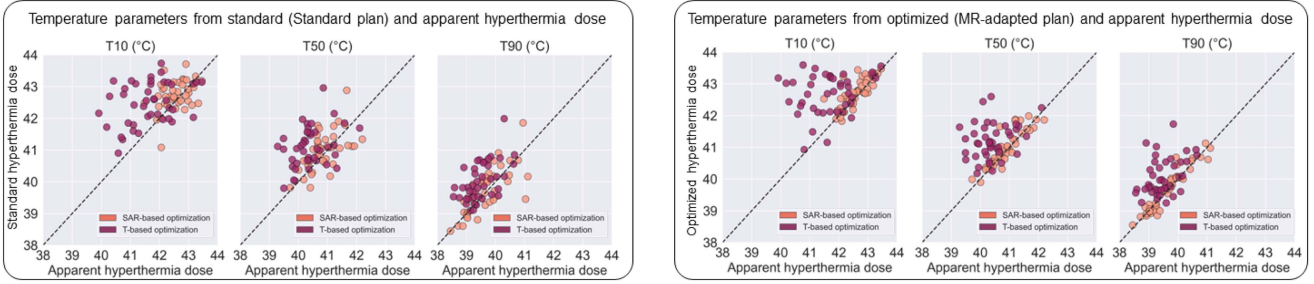
Fig. 5. Scatter plots of the temperature values (T10, T50 and T90) for each optimization and setup. The first set of scatter plots shows the temperature parameters of the standard hyperthermia dose (standard plan) and apparent hyperthermia dose where the volunteer was in the planning setup and treatment setup, respectively. In the second set of scatter plots, temperature parameters were calculated for the optimized hyperthermia dose and apparent hyperthermia dose where in both scenarios the volunteer was in the treatment setup.
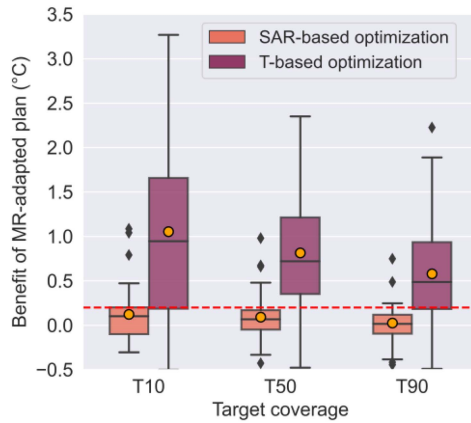
Fig. 6. Boxplot demonstrating the benefit of MR-adapted treatment plan compared to apparent hyperthermia dose using SAR- or T-based optimization. Hence, the difference between the optimized and apparent hyperthermia is demonstrated. The inter-quartile range represents the middle 50% of the dataset where the top line represents 75% of the data below the upper quartile and the bottom line consists of 25% of the data below the lower quartile. The middle line represents the median, the colored circle represents the average of the data set and the diamond shaped markers represent the outliers. The red dotted line denotes the clinically relevant temperature difference (0.2 °C).

and T10 was not clinically relevant (<0.2 °C). In contrast, the benefit of including the treatment anatomy and position for temperature-based optimization leads to improvements higher than 0.5 °C in all temperature metrics. Note that the temperature parameters acquire used to calculate the benefit are illustrated in Fig. 5.

C. Temperature Distributions From One Volunteer

Furthermore, Fig. 7 illustrates the 2D temperature distributions of a volunteer. The same steering settings were used in the standard and apparent hyperthermia doses. For SAR-based optimization, the temperature pattern is similar for standard and apparent hyperthermia doses. On the contrary, for temperature-based optimization, the location of hotspots and target coverage vary significantly between these two doses. Hence, these substantial deviations suggest that temperature-based optimization is more sensitive to changes in anatomy and position. Furthermore, we observed that the temperature in the tumor

is more homogenous resulting in higher target coverage when using temperature-based optimization. Although SAR-based optimization led to lower temperatures in the target region, inferior temperatures were observed in the healthy tissue. The homogeneity (3) and spearing the healthy tissues (2) is strongly related with the optimization function used contributing to how robust the approach is to changes in modelling.

### D. Robustness of the Results Considering Different Perfusion Values

Table II shows that the observations found in the previous sections are robust to different perfusion values: Baseline (Bas), thermal stress A (St. A), and St. B. For both optimization approaches, the absolute error between standard hyperthermia dose and apparent hyperthermia dose were substantial. The benefit of using an MR-adapted plan was clinically relevant when using temperature-based optimization. We found that SAR-based optimization was more robust than temperature-based optimization to changes in anatomy and position since lower variations were observed in benefit and absolute error.

The results suggest that perfusion affects the achieved tumor temperatures. For both optimizations and treatment plans, using the perfusion set St. B led to higher tumor temperatures than the other perfusion sets (Bas. and St. A). The achieved target coverage when using perfusion St. B was 0.10 °C (ΔT10), 0.84 °C (ΔT50) and 0.88 °C (ΔT90) higher compared to the temperatures acquired using perfusion St. A. Perfusion St. B led to 0.94 °C (ΔT10), 0.68 °C (ΔT50), and 0.58 °C (ΔT90) higher temperatures compared to the perfusion at Baseline condition (Bas).

The results in Fig. 8 show that SAR-based optimization is more robust to changes in perfusion than temperature-based optimization since the absolute error and benefit in T50 did not vary substantially. For temperature-based optimization, in both absolute error and benefit, perfusion value St. A led to significant differences (p-values<0.01).

IV. DISCUSSION

Our temperature assessment showed that it is essential to consider the accurate patient anatomy and position when using HTP predictions to guide the treatment. These results highlight
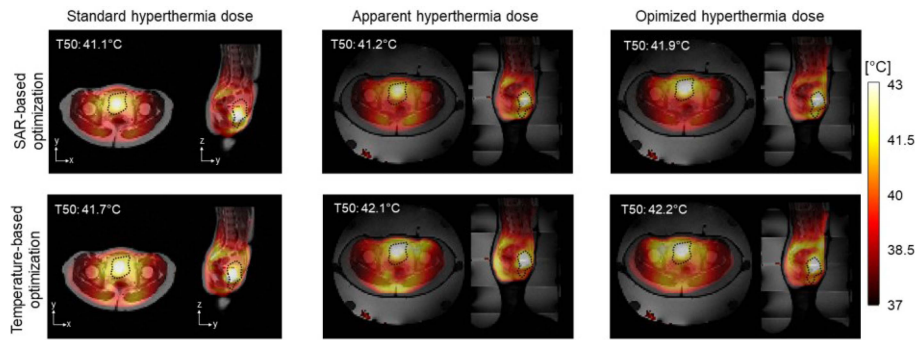
Fig. 7. 2D temperature distributions of a volunteer together with the calculated target coverage (T50). Temperature distributions were acquired using perfusion at thermal stress B. The cross-section represents the same region of the volunteer planning and treatment setup. Between the planning and treatment position, we found a displacement of (0.2 cm, 4.3 cm, 3.4 cm) in (x,y,z). Hence, in the axial cross-section of the standard dose (planning setup), the region denotes the middle slice (z = 0 cm) while in the apparent and optimized hyperthermia dose, the region is 3 cm above (z = +3 cm). The target region in apparent and optimized hyperthermia dose presents a different shape because the volunteer as moved in the z-direction. The dotted line indicates the target region.

TABLE II
AVERAGE AND STANDARD DEVIATION ($\mu \pm \sigma$) OF THE ABSOLUTE ERROR BETWEEN STANDARD HYPERTHERMIA DOSE (STANDARD PLAN) AND APPARENT HYPERTHERMIA DOSE AND THE BENEFIT OF MR-ADAPTED PLAN, CONSIDERING THE THREE PERFUSION SETS

Absolute error between apparent and standard hyperthermia dose					
SAR-based optimization			Temperature-based optimization		
$|\Delta T10|$	$|\Delta T50|$	$|\Delta T90|$	$|\Delta T10|$	$|\Delta T50|$	$|\Delta T90|$
0.42±0.40	0.40±0.38	0.35±0.33	0.89±0.68	0.67±0.53	0.50±0.40
Benefit of MR-adapted plan compared to the apparent hyperthermia dose					
SAR-based optimization			Temperature-based optimization		
$\Delta T10$	$\Delta T50$	$\Delta T90$	$\Delta T10$	$\Delta T50$	$\Delta T90$
0.20±0.32	0.14±0.25	0.07±0.20	0.95±0.81	0.70±0.61	0.50±0.52

The values correspond to 126 treatment plans and corresponding hyperthermia doses administered to 14 volunteers across three tumor sizes and three perfusion sets.
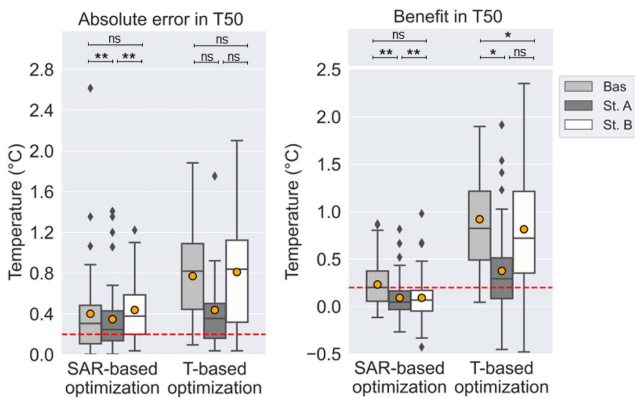
Fig. 8. Boxplot of absolute error and benefit in T50 for each perfusion set using SAR-based and temperature-based optimization. The level of significance is shown in which ns denotes no significance (p>0.05), ∗ denote p-value≤0.05, ∗∗ denotes p-value≤0.01. The inter-quartile range represents the middle 50% of the dataset where the top line represents 75% of the data below the upper quartile and the bottom line consists of 25% of the data below the lower quartile. The middle line represents the median, the colored circle represents the average of the data set and the diamond shaped markers represent the outliers. The red dotted line denotes the clinically relevant temperature difference (0.2 °C). The dataset of each boxplot includes 42 data points (14 volunteers x 3 tumor sizes).

the potential of using MR imaging to create a treatment plan that considers the accurate treatment situation. Based on the large absolute errors illustrated in Table II, capturing the accurate treatment position and anatomy seems more important when the optimization approach is based on temperature. Compared to other studies, we found similar or higher errors when using temperature-based optimization. Gellermann et al. [8] reported that displacements up to 3 cm (as in our study [21]) caused temperature deviations up to ±0.5 °C in $\Delta T90$ using temperature-based optimization. De Greef et al. [33] used temperature-based optimization and found that the changes in tumor temperatures were between 0.3 °C–0.5 °C when the accuracy of patient positioning was within 1-2cm in the z-direction (superior-inferior direction). As shown in our previous study [21], we mainly found position changes in the y-direction (posterior-anterior direction), while these were less than 1cm in the z-direction. We justify the difference by the fact that we included anatomy changes and shifts in the y-direction.

Regarding the benefit of the MR-adapted plan, we found that this plan did not improve the temperatures using SAR-based optimization. In contrast, a clear improvement in tumor temperatures (0.4 °C to 0.7 °C in $\Delta T50$) was observed when using temperature-based optimization. Although the MR-adapted plan benefit was not seen for the two optimization approaches, we

expect that this plan's benefit would be higher in patients. In this volunteer study, the time between the planning and treatment setup was 17 to 20 minutes. Between these two setups, we observed positioning deviations but not substantial anatomical changes. Because patients are imaged several days to weeks before the treatment delivery for HTP, the variations in anatomical configuration of the pelvis region are likely higher than those in our study. Hence, daily anatomic changes are to be expected to be higher, and consequently, a higher benefit when including the accurate anatomy in HTP.

Uncertainties in tissue perfusion pose a great challenge for thermal modelling. Although we observed significant deviations in target temperatures (ΔT50: 0.68 °C to 0.84 °C), due to perfusion variation, we found that the importance of accurate anatomy and positioning remained consistent regardless of these variations. However, application of temperature-based optimization was less robust than SAR-based optimization to changes in perfusion. To understanding the differences in the results, it is important to realize that an optimization approach is considered effective when the desired temperature in the tumor is achieved while avoiding the occurrence of hotspots. The temperature-based optimization was performed for each perfusion scheme, and consequently, the heating was adjusted to the effect of perfusion. Another aspect to consider is that hotspots are dominantly caused in tissue interfaces with high contrast in tissue properties such as muscle/bone and fat/bone. Perfusion set St. A presented the most distinct results because the perfusion contrast (Table I) within the tissues was higher than the other sets ($\omega_{muscle}/\omega_{bone}$=30, $\omega_{muscle}/\omega_{fat}$=1.5). On the contrary, the results suggest that SAR-based optimization made the effect of perfusion redundant likely because this optimization only used the direct absorption and did not consider changes in blood flow [25], making it naturally less sensitive to perfusion differences.

As mentioned before, this study did not intend to clarify if SAR or temperature optimization performs best. Nevertheless, our results highlight the advantages and drawbacks of each approach. The findings suggest that temperature-based optimization might be more effective in providing the desired temperature (Fig. 5) and can be a more patient-specific solution. However, the large uncertainties in perfusion lead to absolute errors of ΔT50 up to 2 °C. In contrast, SAR-based optimization is predicted to be less effective in achieving higher temperatures, but the maximum absolute error was below 1 °C in T50 (Fig. 8 - Interquartile variation <1 °C). Furthermore, as shown in Fig. 6, volunteer displacements had a great impact on the temperature-based optimization since we observed that higher differences in the resulting temperature distribution.

This research showed the value of using MR imaging to achieve a more accurate translation of HTP results and create a treatment plan adapted to the treatment anatomy and position. MR imaging is highly beneficial for MR-compatible devices since it offers the framework to create an HTP for every treatment. Creating a treatment plan right before the treatment requires speeding up HTP (Fig. 3) from approximately 3.5 hours to less than 10 minutes. Reducing the time of HTP is not a trivial task and is still a work in progress, though our research showed that precise repositioning would improve substantially the predictions. Furthermore, perfusion variability affects temperature predictions. In addition, to use MR imaging to facilitate accurate position and anatomy representation, MR methods should be used to improve the accuracy of perfusion modeling [34]. Following this, we believe that using MR imaging during MR-guided hyperthermia is the gateway for more personalized treatment and facilitates much faster progress in understanding the patient's thermal-dose effect relations, thermoregulation, and the need to improve patient positioning.

This study has some weaknesses, and the results should be seen in the light of these considerations. Although we have included perfusion variability, we used static perfusion values and these values, and their dependence on time and temperature, are uncertain themselves. Hence, we believe that future work should focus on improving perfusion modeling for different tissues. Another important aspect to reflect is the goal function and parameters used in the optimization approach. Even though the functions and parameters used in this study are the most commonly adopted and suggested for simulation studies [18], other options have been proposed in literature [25], [35], [36], [37]. Even though the achieved temperatures might change with the goal function, we believe that the observations drawn between the standard plan, the simulated treatment and the adapted plan will hold for optimization using different goal functions.

V. CONCLUSION

Our modeling study suggests that patient anatomy and position during treatment should be taken into account when aiming for accurate thermal simulations; we found absolute errors between 0.40 °C and 0.67 °C in T50. The benefit of MR-adapted HTP was relevant for temperature-based optimization, while for SAR-based optimization, it was less substantial. Furthermore, the findings suggest that SAR-based optimization is more robust to variations in perfusion.

REFERENCES

[1] J. van der Zee, "Heating the patient: A promising approach?," *Ann. Oncol.*, vol. 13, no. 8, pp. 1173–1184, 2002.

[2] P. Wust et al., "Hyperthermia in combined treatment of cancer," *Lancet Oncol.*, vol. 3, no. 8, pp. 487–497, 2002.

[3] M. Franckena et al., "Hyperthermia dose-effect relationship in 420 patients with cervical cancer treated with combined radiotherapy and hyperthermia," *Eur. J. Cancer*, vol. 45, no. 11, pp. 1969–1978, 2009, doi: 10.1016/j.ejca.2009.03.009.

[4] M. Kroesen et al., "Confirmation of thermal dose as a predictor of local control in cervical carcinoma patients treated with state-of-the-art radiation therapy and hyperthermia," *Radiotherapy Oncol.*, vol. 140, pp. 150–158, 2019.

[5] R. A. M. Canters, M. Franckena, M. M. Paulides, and G. C. Van Rhoon, "Patient positioning in deep hyperthermia: Influences of inaccuracies, signal correction possibilities and optimization potential," *Phys. Med. Biol.*, vol. 54, no. 12, pp. 3923–3936, 2009.

[6] M. Franckena, R. Canters, F. Termorshuizen, J. Van Der Zee, and G. Van Rhoon, "Clinical implementation of hyperthermia treatment planning guided steering: A cross over trial to assess its current contribution to treatment quality," *Int. J. Hyperth ermia*, vol. 26, no. 2, pp. 145–157, 2010.

[7] J. Gellermann et al., "Comparison of MR-thermography and planning calculations in phantoms," *Med. Phys.*, vol. 33, no. 10, pp. 3912–3920, 2006.

[8] J. Gellermann et al., "Simulation of different applicator positions for treatment of a presacral tumour," *Int. J. Hyperthermia*, vol. 23, no. 1, pp. 37–47, 2007.

[9] R. A. M. Canters, M. M. Paulides, M. Franckena, J. W. Mens, and G. C. Van Rhoon, "Benefit of replacing the Sigma-60 by the Sigma-Eye applicator: A Monte Carlo-based uncertainty analysis," *Int. J. Radiat. Oncol. Biol. Phys.*, vol. 189, no. 1, pp. 74–80, 2013.

[10] M. De Greef, H. P. Kok, D. Correia, A. Bel, and J. Crezee, "Optimization in hyperthermia treatment planning: The impact of tissue perfusion uncertainty," *Med. Phys.*, vol. 37, no. 9, pp. 4540–4550, 2010.

[11] J. Lang, B. Erdmann, and M. Seebass, "Impact of nonlinear heat transfer on temperature control in regional hyperthermia," *IEEE Trans. Biomed. Eng.*, vol. 46, no. 9, pp. 1129–1138, Sep. 1999, doi: 10.1109/10.784145.

[12] M. De Greef, H. P. Kok, D. Correia, P. P. Borsboom, A. Bel, and J. Crezee, "Uncertainty in hyperthermia treatment planning: The need for robust system design," *Phys. Med. Biol.*, vol. 56, no. 11, pp. 3233–3250, 2011.

[13] C. A. T. Van Den Berg et al., "Towards patient specific thermal modelling of the prostate," *Phys. Med. Biol.*, vol. 51, no. 4, pp. 809–825, 2006, doi: 10.1088/0031-9155/51/4/004.

[14] F. Khalifa et al., "Models and methods for analyzing DCE-MRI: A review," *Med. Phys.*, vol. 41, no. 12, 2014, Art. no. 124301, doi: 10.1118/1.4898202.

[15] L. Lüdemann, P. Wust, and J. Gellermann, "Perfusion measurement using DCE-MRI: Implications for hyperthermia," *Int. J. Hyperthermia*, vol. 24, no. 1, pp. 91–96, 2008, doi: 10.1080/02656730701836954.

[16] R. A. M. Canters, M. M. Paulides, M. F. Franckena, J. Van Der Zee, and G. C. Van Rhoon, "Implementation of treatment planning in the routine clinical procedure of regional hyperthermia treatment of cervical cancer: An overview and the Rotterdam experience," *Int. J. Hyperthermia*, vol. 28, no. 6, pp. 570–581, 2012.

[17] E. Burchardt and A. Roszak, "Hyperthermia in cervical cancer – current status," *Rep. Pract. Oncol. Radiotherapy*, vol. 23, no. 6, pp. 595–603, 2018, doi: 10.1016/j.rpor.2018.05.006.

[18] M. M. Paulides et al., "ESHO benchmarks for computational modeling and optimization in hyperthermia therapy," *Int. J. Hyperthermia*, vol. 38, no. 1, pp. 1425–1442, 2021, doi: 10.1080/02656736.2021.1979254.

[19] J. Gellermann et al., "Methods and potentials of magnetic resonance imaging for monitoring radiofrequency hyperthermia in a hybrid system," *Int. J. Hyperthermia*, vol. 21, no. 6, pp. 497–513, 2005.

[20] F. Adibzadeh, K. Sumser, S. Curto, D. T. B. Yeo, A. A. Shishegar, and M. M. Paulides, "Systematic review of pre-clinical and clinical devices for magnetic resonance-guided radiofrequency hyperthermia," *Int. J. Hyperthermia*, vol. 37, no. 1, pp. 15–27, 2020.

[21] I. VilasBoas-Ribeiro, M. Franckena, G. C. van Rhoon, J. A. Hernández-Tamames, and M. M. Paulides, "Using MRI to measure position and anatomy changes and assess their impact on the accuracy of hyperthermia treatment planning for cervical cancer," *Int. J. Hyperthermia*, vol. 40, no. 1, 2022, Art. no. 2151648, doi: 10.1080/02656736.2022.2151648.

[22] H. H. Pennes, "Analysis of tissue and arterial blood temperatures in resting Human forearm," *J. Appl. Physiol.*, vol. 1, no. 2, pp. 1865–1871, 1948.

[23] P. Hasgall et al., "IT'IS database for thermal and electromagnetic parameters of biological tissues," IT'IS Found., 2011. [Online]. Available: itis.swiss/database

[24] Z. Rijnen et al., "Clinical integration of software tool VEDO for adaptive and quantitative application of phased array hyperthermia in the head and neck," *Int. J. Hyperthermia*, vol. 29, no. 3, pp. 181–193, 2013.

[25] R. A. M. Canters, P. Wust, J. F. Bakker, and G. C. Van Rhoon, "A literature survey on indicators for characterisation and optimisation of SAR distributions in deep hyperthermia, a plea for standardisation," *Int. J. Hyperthermia*, vol. 25, no. 7, pp. 593–608, 2009.

[26] H. P. Kok, P. M. A. Van Haaren, J. B. Van De Kamer, J. Wiersma, J. D. P. Van Dijk, and J. Crezee, "High-resolution temperature-based optimization for hyperthermia treatment planning," *Phys. Med. Biol.*, vol. 50, no. 13, pp. 3127–3141, 2005, doi: 10.1088/0031-9155/50/13/011.

[27] H. P. Kok et al., "Prospective treatment planning to improve locoregional hyperthermia for oesophageal cancer," *Int. J. Hyperthermia*, vol. 22, no. 5, pp. 375–389, 2006, doi: 10.1080/02656730600760149.

[28] G. Bruggmoser et al., "Quality assurance for clinical studies in regional deep hyperthermia," *Strahlentherapie und Onkol*, vol. 187, no. 10, pp. 605–610, 2011, doi: 10.1007/s00066-011-1145-x.

[29] M. Franckena et al., "Radiotherapy and hyperthermia for treatment of primary locally advanced cervix cancer: Results in 378 patients," *Int. J. Radiat. Oncol. Biol. Phys.*, vol. 73, no. 1, pp. 242–250, 2009, doi: 10.1016/j.ijrobp.2008.03.072.

[30] R. F. Verhaart, V. Fortunati, G. M. Verduijn, T. Van Walsum, J. F. Veenland, and M. M. Paulides, "CT-based patient modeling for head and neck hyperthermia treatment planning: Manual versus automatic normal-tissue-segmentation," *Radiotherapy Oncol.*, vol. 111, no. 1, pp. 158–163, 2014.

[31] G. Sreenivasa et al., "Clinical use of the hyperthermia treatment planning system HyperPlan to predict effectiveness and toxicity," *Int. J. Radiat. Oncol. Biol. Phys.*, vol. 55, no. 2, pp. 407–419, 2003.

[32] R. F. Verhaart et al., "Temperature simulations in hyperthermia treatment planning of the head and neck region," *Strahlentherapie und Onkol*, vol. 190, no. 12, pp. 1117–1124, 2014.

[33] M. De Greef, H. P. Kok, A. Bel, and J. Crezee, "3D versus 2D steering in patient anatomies: A comparison using hyperthermia treatment planning," *Int. J. Hyperthermia*, vol. 27, no. 1, pp. 74–85, 2011.

[34] L. C. Sebeke et al., "Visualization of thermal washout due to spatiotemporally heterogenous perfusion in the application of a model-based control algorithm for MR-HIFU mediated hyperthermia," *Int. J. Hyperthermia*, vol. 38, no. 1, pp. 1174–1187, 2021.

[35] H. P. Kok, A. N. T. J. Kotte, and J. Crezee, "Planning, optimisation and evaluation of hyperthermia treatments," *Int. J. Hyperthermia*, vol. 33, no. 6, pp. 593–607, 2017.

[36] A. Kuehne, E. Oberacker, H. Waiczies, and T. Niendorf, "Solving the time- and frequency-multiplexed problem of constrained radiofrequency induced hyperthermia," *Cancers (Basel)*, vol. 12, no. 5, 2020, Art. no. 1072, doi: 10.3390/cancers12051072.

[37] M. Zanoli and H. Dobšíček Trefná, "The hot-to-cold spot quotient for SAR-based treatment planning in deep microwave hyperthermia," *Int. J. Hyperthermia*, vol. 39, no. 1, pp. 1421–1439, 2022, doi: 10.1080/02656736.2022.2136411.